

# Discovery of new *TESS* pulsating hot subdwarfs

J. Krzesinski<sup>1</sup> and L. A. Balona<sup>2</sup>

<sup>1</sup> Astronomical Observatory, Jagiellonian University, ul. Orła 171, PL-30-244 Krakow, Poland  
e-mail: jk@oa.uj.edu.pl

<sup>2</sup> South African Astronomical Observatory, P.O. Box 9, Observatory, Cape Town, South Africa  
e-mail: labsaao.ac.za

Received 2021

## ABSTRACT

**Aims.** This work is dedicated to a search for new pulsating hot subdwarfs in *TESS* photometric data which could have been missed in previous searches.

**Methods.** By matching catalogues of hot subdwarfs with *TESS* targets and using luminosities from *Gaia* parallaxes, a list of 1389 candidate hot subdwarfs observed by *TESS* was created. The periodograms of these stars were inspected, and the stars were classified according to variability type.

**Results.** An updated catalogue of all known pulsating hot subdwarfs is presented. A number of probable pulsating binaries have been identified, which might prove useful for verifying the asteroseismic masses. The mean masses of p- and g-mode pulsators are estimated from the stellar parameters.

**Conclusions.** A list of 63 previously unknown pulsating hot subdwarfs observed by *TESS* is presented. More than half of the stars previously identified as pure p-mode pulsators are found to have frequencies in the g-mode region as well. As a result, hybrid p- and g-mode pulsators occur over the whole instability strip.

**Key words.** stars:subdwarfs; stars:oscillations;

## 1. Introduction

Hot subdwarf stars form roughly two classes of objects. The cooler subdwarf B-type (sdB) class, whose spectra typically show no or weak helium lines, and the hotter subdwarf O-type (sdO) class, which has (on average) a higher helium abundance (Stroeer et al. 2007).

The sdBs are core He-burning stars on the extreme horizontal branch having very thin hydrogen envelopes (Heber 1986; Saffer et al. 1994; Heber 2016). It is thought that most of the hydrogen was removed by mass loss that could have occurred as a result of mass interchange in a binary system (Han et al. 2002, 2003). This is supported by the fact that many sdB stars are close binary systems, which are either late M-type main sequence stars or white dwarfs (Maxted et al. 2001; Heber 2016). The effective temperature range of the sdBs is between 20 000 and 40 000 K and the surface gravity ( $\log g$ ) is between 5.2 and 6.2 (Green et al. 2008; Saffer et al. 1994).

The hotter sdO class encompasses a wider range of hot objects with diverse origins. These stars are located blueward of the extreme horizontal branch stars in the HR diagram (Stroeer et al. 2007; Németh et al. 2012). Most are likely descendants of red giant stars; however, a few have luminosities and temperatures similar to the central stars of planetary nebulae and therefore might be of post-AGB origin (Heber et al. 1988; Rauch et al. 1991). Because evolutionary tracks of sdB stars pass through the sdO region (Dorman et al. 1993), a link between the two classes is also possible and some sdOs in the class might also be descendants of sdB stars. On the other hand, the population of sdO stars consists mostly of single stars (Napiwotzki 2008); therefore, a merger of two helium white dwarfs (Webbink 1984; Iben & Tutukov 1984; Saio & Jeffery 2000), and the de-

layed helium flash of a WD (Lanz et al. 2004) or hot-flasher (Miller Bertolami et al. 2008) were the scenarios suggested to explain the existence of some of these stars.

The effective temperatures of the hotter sdOs can reach up to 80 000 K, and due to the diversity of the sdO stars, their surface gravity ( $\log g$ ) range (4.0 – 6.5) is broader than for sdBs (Oreiro Rey et al. 2004; Johnson et al. 2014; Heber 2009, 2016). The fraction of sdO stars with temperatures around 40 000 K are likely He-burning subdwarfs, while the hotter sdOs are thought to have entered a subsequent He-shell-burning phase (Wang et al. 2021). For an in-depth review of the two classes, see Heber (2016).

Charpinet et al. (1996) investigated pulsational driving in sdB stars. They found that most of the driving is the result of the opacity  $\kappa$ -mechanism operating in the partial ionisation zone of Fe-group elements. This is the same mechanism that operates in the main sequence  $\beta$  Cep and SPB stars (Moskalik & Dziembowski 1992; Dziembowski et al. 1993). However, pulsation in models of sdB stars will only occur if the metal abundance in the driving region is enhanced by about a factor of two at uniform envelope abundance. A basic result of radiatively driven diffusion is that an element accumulates in a layer where the specific opacity for the element is highest. Therefore, Fe-group elements will tend to be enhanced in the region of the opacity bump, as required for pulsational driving.

Shortly after these model calculations, Kilkeny et al. (1997) reported the discovery of small-amplitude, rapid light variations in the sdB binary, EC 14026-2647. The main frequency peak is at about  $600 \text{ d}^{-1}$  with an amplitude of about 0.01 mag. Since then, many other sdB stars pulsating at high frequencies have been discovered. These p-mode pulsators are now called the V361 Hya variables.

Green et al. (2003) discovered a second family of related sdB stars. These are also low-amplitude multiperiodic variables, but with frequencies in the range  $10\text{--}50\text{ d}^{-1}$ . These are called V1093 Her variables. The pulsations are attributed to g-modes of low spherical harmonic degree driven by the same mechanism as in the hotter V361 Hya stars (Fontaine et al. 2003). Because they have lower effective temperatures, the driving zone is deeper in the V1093 Her stars and the thermal timescale is longer. As a result, only g-mode pulsations of long periods are unstable. The situation is analogous to the  $\beta$  Cep/SPB case.

It should be mentioned that pulsating stars have also been found among sdOs. The first in this class is SDSS J160043.6+074802.9, a subdwarf discovered by Woudt et al. (2007); it is a binary with a late-type companion (Rodríguez-López et al. 2010). The second, previously classified as a sdBV in a binary system with an F0 star (Koen et al. 1997; O’Donoghue et al. 1998), is EO Cet (PB8783), which was later re-classified as an sdO pulsator (Østensen 2012). The last is EC 03089-6421, a sdOV star discovered by Kilkenny et al. (2017). All are rapid pulsators with periods in the range 0.5 – 2 minutes. There were also cooler ( $\sim 50\,000\text{ K}$ ) sdO pulsators discovered in a globular cluster ( $\omega$  Cen) (Randall et al. 2011, 2016), but they likely make up a different class of subdwarf pulsators than the field sdOV stars.

Space photometry from the *Kepler* mission (Borucki et al. 2010) and from the *TESS* mission (Stassun et al. 2019) has been an important source of new candidates for V1093 Her and V361 Hya classes of variables (Østensen et al. 2010b, 2011; Kawaler et al. 2010b,a; Reed et al. 2010). The majority of the sdB stars observed by *Kepler* are V1093 Her variables (16 stars), with one hybrid and one V361 Hya star. Analysis of data from the extended *Kepler K2* mission resulted in the discovery of 15 pulsating sdB variables, two of which belong to the V361 Hya class (Reed et al. 2018b). Analysis of data from the *TESS* mission is ongoing (Reed et al. 2020; Uzundag et al. 2021; Sahoo et al. 2020a; Charpinet et al. 2019). Holdsworth et al. (2017) gives a table of 110 pulsating subdwarfs known at the time. Lynas-Gray (2021) presents a good review which includes a list of 56 known pulsating sdB stars.

More recently, Van Grootel et al. (2021) has presented three lists of 1302, 269, and 1013 confirmed hot subdwarfs (including hot subdwarf pulsators) observed by the *TESS* mission. These numbers are taken from their online catalogues (see link in their paper). These catalogues were assembled by Working Group 8 (WG8, compact pulsators) of the *TESS Asteroseismic Consortium*. Their contents overlap, so that the total number of entries is larger than the actual number of hot subdwarfs.

In this paper we present the results of a search for pulsating hot subdwarfs using *TESS* photometry. We begin in Section 2 by describing the *TESS* data and how hot subdwarfs are identified. We emphasize the importance of *Gaia* parallaxes (Gaia Collaboration et al. 2016, 2018) in this regard. In Section 3 we discuss lists of known hot subdwarf pulsators and why it is important to identify p- and g-mode pulsators. In Section 4 the search for variability among *TESS* stars identified as probable hot subdwarfs is discussed. The criteria used to distinguish between eclipsing and pulsating stars from the periodograms is described. The effect of contamination from nearby stars is discussed. The mass distribution of hot subdwarfs derived from *Gaia* luminosities and published surface gravities is discussed in Section 5. This allows the relative masses of p- and g-mode pulsating hot subdwarfs to be estimated. In Section 6 the location of the pulsating hot subdwarfs in the Hertzsprung–Russell (H–R) diagram is discussed and compared to the models. In the

Appendix a catalogue of all known pulsating hot subdwarfs discovered since the previous listing by Holdsworth et al. (2017) is presented. A table of the newly discovered pulsating hot subdwarfs is also presented. A separate list of many new pulsating hot subdwarfs, which were unrecognized as pulsators by Van Grootel et al. (2021), is included. Finally, the periodograms of all newly discovered pulsating hot subdwarfs are shown.

## 2. Data and identification of hot subdwarfs

The *TESS* photometric survey consists of continuous wide-band photometry of 13 sectors per celestial hemisphere (Ricker et al. 2014). Each sector is observed continuously for about 27 days with 2 min cadence. Stars near the ecliptic equator are only observed for one sector. Stars nearer the poles may be observed in more than one sector so that, at the ecliptic poles, stars are observed continuously for over 350 days. The light curves are corrected for time-correlated instrumental signatures using pre-search data conditioning (PDC, Jenkins et al. 2016). These are the data labelled PDCSAP\_FLUX in the light curve FITS files. The data used here are the full PDCSAP light curves from sectors 1–38. As this was part of a survey for stellar variability among many thousands of *TESS* stars, no effort was made to optimise the aperture. The light curves for *TESS* stars are available on the *MAST* website (<https://archive.stsci.edu/>).

Hot subdwarfs were first identified in surveys of faint blue stars at high Galactic latitudes (Humason & Zwicky 1947). Subsequent surveys added to the list. The first catalogue of spectroscopically identified hot subdwarf stars (Kilkenny et al. 1988) contained 1225 sdB and sdO stars. Østensen (2006) expanded the list to more than 2300 stars. The advent of mass surveys such as the Sloan Digital Sky Survey (SDSS) extended the search to fainter magnitudes and provided spectra of almost 2000 hot subdwarfs (Geier et al. 2015; Kepler et al. 2015, 2016). The precise proper motions and parallaxes provided by *Gaia* (Gaia Collaboration et al. 2016, 2018) has led to an even greater number of possible subdwarf candidates based on colour, absolute magnitude, and reduced proper motion cuts (Geier et al. 2017a, 2019; Geier 2020).

These lists were cross-matched with the *TESS* input catalogue (Stassun et al. 2019), leading to 1398 hot subdwarf candidates for which light curves are available. Not surprisingly, the majority of these stars are also listed on the WG8 list of compact pulsators.

Perhaps the most direct way of identifying hot subdwarfs is to place the star in the H–R diagram. The photometric effective temperatures for hot stars are unreliable unless they include observations in the UV band. The sources of effective temperature,  $T_{\text{eff}}$ , are mainly those in Geier (2020), but the literature was searched for further values using the *SIMBAD* database (Wenger et al. 2000) for stars of interest. The luminosity for each star was estimated from *Gaia* EDR3 parallax (Gaia Collaboration et al. 2016, 2018) in conjunction with reddening obtained from a three-dimensional map by Gontcharov (2017) using the bolometric correction calibration by Pecaut & Mamajek (2013). From the error in the *Gaia* parallax, the typical standard deviation in  $\log(L/L_{\odot})$  is estimated to be about 0.10 dex, allowing for standard deviations of 0.1 mag in the apparent magnitude, 0.1 mag in visual extinction and 0.1 mag in the bolometric correction in addition to the parallax error.

Unfortunately, the effective temperature is not available for many stars. It turns out that the derived luminosity is only slightly dependent on  $T_{\text{eff}}$ , which is mainly used for deriving the bolometric correction. On the assumption that the selected stars

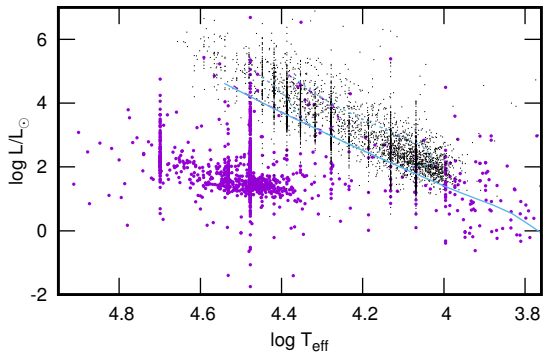


**Fig. 1.** Theoretical H–R diagram showing subdwarfs (violet filled circles) and main sequence stars brighter than 12.5 mag (small black circles) observed by *TESS*. Luminosities were derived from *Gaia* parallaxes. The vertical arraignment of some points is due to adopted values of  $T_{\text{eff}} = 50000$  K for sdO and  $T_{\text{eff}} = 30000$  K for sdB stars for which values are not available and the use of  $T_{\text{eff}}$  from spectral types for some main sequence stars. The solid line is the zero age main sequence for models with solar abundance (Bertelli et al. 2008). Also shown are the theoretical instability strips for  $\beta$  Cep and SPB stars from Miglio et al. (2007).

are subdwarfs, a good approximation to the luminosity for stars without effective temperature measurements can be obtained simply by adopting  $T_{\text{eff}} \approx 30000$  K for sdB and  $T_{\text{eff}} \approx 50000$  K for sdO stars. The approximate luminosity obtained in this way is a good indicator of whether or not the star is a subdwarf. Figure 1 shows the theoretical H–R diagram for all *TESS* subdwarf candidates for which parallaxes are available.

As can be seen, there are some stars well above the subdwarf sequence. Stars with  $\log(L/L_{\odot})$  exceeding approximately 1 dex above the well-defined subdwarf sequence were eliminated from the sample. There are also several stars cooler than about 15000 K. The effective temperatures for these stars are nearly all derived from photometric indices and are considered unreliable. On the assumption that they are all subdwarfs, and assigning  $T_{\text{eff}} = 30000$  K to these stars, some were found to have luminosities consistent with hot subdwarfs. As a result, of the 1389 *TESS* subdwarf candidates examined, about 1250 lie within the hot subdwarf region. These stars were retained for further study, while the others were rejected.

### 3. Known hot subdwarf pulsators

Since the last compilation by Holdsworth et al. (2017), several studies have identified more pulsating hot subdwarfs. A list of these additional V361 Hya and V1093 Her stars is given in Table A1 in the Appendix. More recently, Van Grootel et al. (2021) have identified new pulsating hot subdwarfs using *TESS* photometry. These are also included in Table A1. Wherever possible, effective temperatures from the literature are included in the tables. Where no effective temperatures are available, the adopted effective temperatures described above were used to estimate the luminosity.

There are 26 known pure p-mode pulsators observed by *TESS* in the compilation by Holdsworth et al. (2017). In ten of these stars significant frequency peaks in the g-mode region were detected (Fig. 2). These stars, listed in Table 1, clearly need to be re-classified as p+g-mode hybrids. In this table, a list of previously unrecognised sdBV binary candidates is also given.

The only meaningful subdivision of sdBV stars is the classification into p-mode and g-mode variables. The restoring force

**Table 1.** Stars in Holdsworth et al. (2017) classified as pure p-mode pulsators but which have clear g-mode frequency peaks in the *TESS* photometry. In the second half of the table, known sdBV stars are listed in which binary variation may be present. Effective temperatures are from Holdsworth et al. (2017) and spectral types from the literature.

TIC Name	$T_{\text{eff}}$ (kK)	$\log(L/L_{\odot})$	Sp. Type
p-mode sdBV reclassified as hybrid pulsators:			
47377536	$35.0 \pm 1.0$	$1.59 \pm 0.07$	sdO9VHe6
62381958	$37.1 \pm 0.3$	$1.52 \pm 0.08$	sdO/Bsd+MSsdB
62483415	$35.1 \pm 0.3$	$1.46 \pm 0.07$	sdO/BsdO/BsdO
95752908	$34.2 \pm 0.5$	$1.28 \pm 0.07$	sdB
136975077	$31.8 \pm 0.6$	$1.50 \pm 0.07$	sdBV
138618727	$29.5 \pm 0.2$	$1.58 \pm 0.07$	sdBV+dM
142200764	$31.6 \pm 0.5$	$1.62 \pm 0.08$	sdB+dM
165312944	$33.7 \pm 0.3$	$1.46 \pm 0.07$	sdBV
396954061	$34.0 \pm 0.5$	$1.45 \pm 0.07$	sdBV
434923593	$28.5 \pm 0.7$	$1.20 \pm 0.07$	sdBV+dM,
New binary candidates:			
80290366	$25.2 \pm 1.2$	$1.38 \pm 0.07$	sdBV
80427831		$1.29 \pm 0.08$	sdB+WD
117070953	$170.0 \pm 2.0$	$1.76 \pm 0.07$	
115280751	$32.4 \pm 0.3$	$1.93 \pm 0.10$	sdBV+G0
137608661		$1.41 \pm 0.07$	sdB
138618727	$29.5 \pm 0.2$	$1.58 \pm 0.07$	sdBV+dM
142200764	$31.6 \pm 0.5$	$1.62 \pm 0.08$	sdB+dM
175402069	$31.4 \pm 0.2$	$1.32 \pm 0.07$	sdBV+dM
220573709	$52.0 \pm 3.0$	$1.61 \pm 0.07$	sdO
352480413	$25.4 \pm 0.3$	$1.38 \pm 0.07$	sdB+dM
436579904	$32.0 \pm 0.4$	$1.24 \pm 0.07$	sdBV+dM

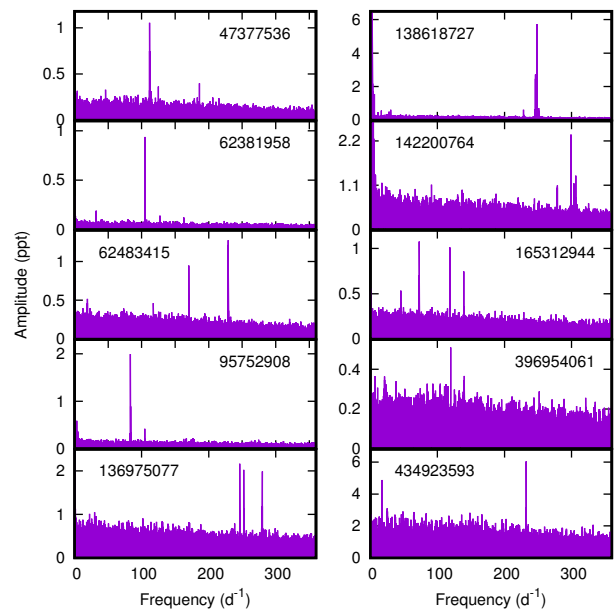


**Fig. 2.** Known pure p-mode pulsating hot subdwarfs observed by *TESS* showing frequency peaks in the g-mode range.

in p-mode variables is the pressure, while for g-mode variables it is buoyancy. The subdivision is based on the expected frequency ranges for p- and g-modes derived from models. The theoretical pulsation period boundary between p- and g-modes is around 250 s or a frequency of  $340 \text{ d}^{-1}$  (Bloemen et al. 2014). This is the criterion used by Holdsworth et al. (2017). In this paper we use this definition of p- and g-mode variables. The shortest period that can be observed by *TESS* is 240 s (2 min cadence), which means that only g-mode pulsators (V1096 Her stars) can be detected.

#### 4. New pulsational variables

The *TESS* periodograms of hot subdwarfs have relatively low signal-to-noise ratios owing to the faintness of the stars. It should also be noted that the *TESS* photometric bandpass is very wide and mostly sensitive in the near infrared (Ricker et al. 2014). This is not well suited to detecting pulsations in very hot stars because the amplitudes are much lower in the near infrared than in the blue region of the spectrum.

The periodograms of each star were visually inspected and the type of variability noted. Any star in which only one peak below  $30 \text{ d}^{-1}$  or a peak with one or more harmonics was detected is regarded as a binary. The dips in the light curves of detached eclipsing binaries manifest as harmonics in the periodogram. The possibility exists that the variability is due to pulsation modes with harmonics or even rotation, rather than binarity. The differences cannot be distinguished from the light curve alone. On the other hand, if multiple peaks are seen that are not in a harmonic relation, then one may feel confident that pulsation is involved.

In a few stars, a frequency peak with one or more harmonics is present in addition to other unrelated frequency peaks. These stars are classified as possible pulsating binary hot subdwarfs.

No significant light variation could be seen in 640 stars. There are 24 stars that are clearly main sequence stars with erroneous parallaxes, and 12 stars with irregular light variations. As many as 410 possible binaries were noted, but half of them have uncertain low amplitudes. We classified 210 stars as definite binary candidates, 8 of which were noted to have flares (presumably originating in a cool companion).

Inspection of the periodograms of the *TESS* candidates within the sdB region of the H–R diagram showed many of the variables have only a single significant peak in the periodogram. These stars were removed from the sdBV candidate list on the assumption that the periodicity might be due to binary motion rather than pulsation, as described above. After removing a few other stars where the evidence for pulsation was considered too weak, 63 previously unknown pulsating hot subdwarf candidates remain. These include 38 stars in Van Grootel et al. (2021), which seemed to have been overlooked as sdBV stars. They are listed in Table A2 and their periodograms shown in Fig. A1. The remaining 25 stars are newly discovered sdBV candidates (Table A3). Periodograms of these stars are shown in Fig. A2.

*TESS* images of every target star listed in Tables A2 and A3 were visually examined for the presence of background or neighbouring stars that could affect the signal in the *TESS* aperture. The target CCD pixel images were overlaid with scaled SDSS or *Digital Sky Survey* (DSS) images. A visual assessment was made and the probable affect on the light curve designated by the code shown in Tables A2 and A3. The *TESS* pixel is  $21 \times 21$  arcsec and in the worst case (code 3), intrusion of light from neighbouring stars of comparable brightness will affect the measured light amplitude.

Whenever doubts have arisen about light intrusion into the *TESS* aperture, the neighbouring stars were examined for light variability when possible. None of these neighbouring stars appeared to be a variable, but there were some cases where background stars occupied the same pixel as, or an adjoining pixel to the target star. In these cases the field was examined using SDSS or DSS colour images to estimate the colours of the neighbouring stars. In all cases the target appeared to be a blue star, while the neighbour(s) were distinctly cooler. This makes it less likely that the intruding star(s) are responsible for any of the pulsation patterns seen in the hot subdwarfs.

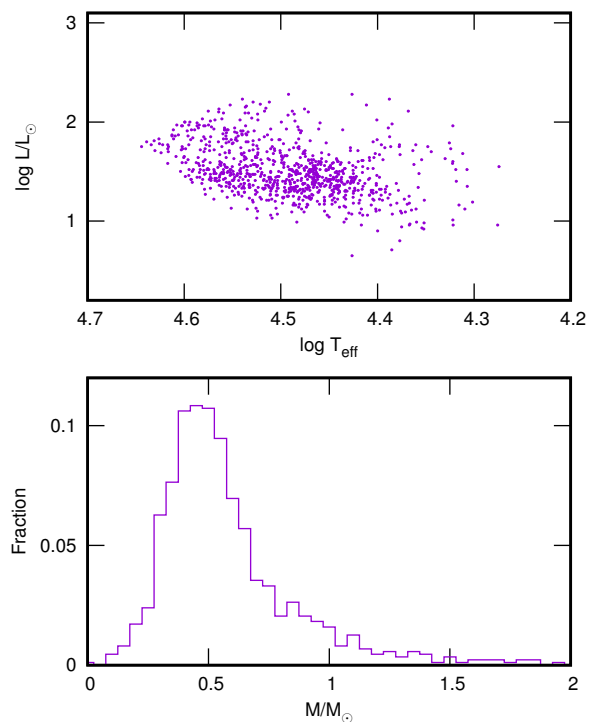


**Fig. 3.** Theoretical H–R diagram of hot subdwarfs extracted from the catalogue of Geier (2020) and located within the instability region (top panel). Bottom panel: Mass distribution of these stars estimated directly from the stellar parameters.

#### 5. Masses

The luminosity derived from *Gaia* parallax provides an independent method of estimating the stellar mass. From the equations  $L/L_{\odot} = (R/R_{\odot})^2 (T_{\text{eff}}/T_{\text{eff}\odot})^4$  and  $g/g_{\odot} = M/M_{\odot} / (R/R_{\odot})^2$  we have

$$\log(M/M_{\odot}) = \log g + \log L/L_{\odot} - 4 \log T_{\text{eff}} + 10.610.$$

Since the  $\log g$ ,  $\log L/L_{\odot}$ , and  $\log T_{\text{eff}}$  values are known for many hot subdwarfs, it is possible to obtain individual stellar masses. These masses might not be reliable because of the large errors in measuring these three quantities. The typical standard deviations are  $\sigma(\log T_{\text{eff}}) \approx 0.010$ ,  $\sigma(\log L/L_{\odot}) \approx 0.011$ ,  $\sigma(\log g) \approx 0.07$  which gives  $\sigma(\log M/M_{\odot}) \approx 0.14$ . The expected error in mass is a substantial fraction of the mass itself. Clearly, obtaining individual stellar masses in this way is not useful. However, the average mass of a fairly large population will be quite well determined and might prove interesting.

The catalogue of Geier (2020) was used to extract 876 candidate subdwarfs with known stellar parameters within the region of the p-mode and g-mode pulsators (top panel of Fig. 3). The bottom panel of Fig. 3 shows the mass distribution of these stars estimated from the above equation. There is a long tail of high masses which could be a result of inclusion of main sequence stars in the Geier (2020) catalogue. There are certainly a number of Be and other peculiar stars in the catalogue. The peak of the distribution is at  $M = 0.45 M_{\odot}$ . If only stars in the range  $0.25 < M/M_{\odot} < 1.0$  are retained, the mean is  $M = 0.545 \pm 0.006 M/M_{\odot}$  from 754 stars.

Among the 754 stars there are 45 g-mode pulsators with mean mass  $M/M_{\odot} = 0.53 \pm 0.02$ . The 11 hybrids have  $M/M_{\odot} = 0.58 \pm 0.04$ , while the 27 p-mode pulsators have a mean mass  $M/M_{\odot} = 0.64 \pm 0.04$ . These values assume that the measured

values of effective temperature, luminosity, and surface gravity are free of systematic errors. Even if the actual values suffer from systematic errors in the measured quantities, the relative values should remain about the same. It is therefore safe to assume that p-mode pulsators have higher masses than g-mode pulsators.

Perhaps the most precise masses are those obtained from asteroseismology (see Fontaine et al. 2012). From 20 asteroseismic masses of p-mode stars the mean mass is  $\overline{M/M_{\odot}} = 0.52 \pm 0.02$ . There are only three g-mode pulsators with asteroseismic masses, giving  $\overline{M/M_{\odot}} = 0.48 \pm 0.01$ . Again, the p-mode pulsators have higher masses, but one can argue that a sample of three g-mode stars is too small for a meaningful determination. On the other hand, the Van Grootel et al. (2013) dynamical and asteroseismic mass determination of PG1336-018, a sdBV in a binary system, seems to confirm the precision of asteroseismological models. The systematic difference between the asteroseismic masses and the masses derived here could be explained if the effective temperatures are increased by about 5%.

In our list of newly discovered pulsating hot subdwarfs, there are ten probable binaries, four of which have between 7 and 13 frequency peaks (Table 1). It might be possible to obtain both pulsation masses and dynamical masses from these stars. This would allow an important verification of the pulsation masses.

## 6. Location of the g-mode hot limit

The models of Fontaine et al. (2003), which can account for the high pulsation frequencies in V386 Hya stars, require the observed modes to be of relatively high degree (spherical harmonic  $l = 3$  or 4) because the more visible low-degree modes are only excited in stars cooler than the coolest known sdB stars. Furthermore, the hot end of the g-mode instability strip turns out to be about  $T_{\text{eff}} \approx 24500$  K, which is significantly cooler than observations.

The discrepancy between the observed and theoretical blue edges was resolved by Jeffery & Saio (2006) using updated opacities together with enhanced Ni and Fe in the driving zone. They find the blue edge at around  $T_{\text{eff}} \approx 28000$  K for  $l = 3$  if the Ni abundance is enhanced by a factor of 20. Hu et al. (2009) found that helium settling causes a shift in the theoretical blue edge of the g-mode instability domain to higher effective temperatures. A blue edge at about  $T_{\text{eff}} \approx 29500$  K is possible for  $l = 3$  modes with Ni enhancement and helium settling.

Bloemen et al. (2014) point out that the abundance enhancements of Fe and Ni due to diffusion were previously underestimated. Their models predict g-mode pulsations at effective temperatures as high as  $T_{\text{eff}} = 33500$  K which is hotter than the observed hot limit for g-modes and well inside the p-mode region.

The top panel of Fig. 4 shows the location of the pulsating hot subdwarfs observed by *TESS* in the H–R diagram. The middle panel shows all known pulsating hot subdwarfs as well as the four blue edges discussed above. As already mentioned, many of the known p-mode *TESS* stars in the literature show distinct frequency peaks in the g-mode region as well (Table 1 and Fig. 2). These new hybrid pulsators, as well as previously known hybrid pulsators, are shown in the middle panel of Fig. 4. They no longer form a tight sequence between the p- and g-mode pulsators, but are to be found right across the instability strip. The bottom panel of Fig. 4 shows the same stars in the more frequently used  $\log g - T_{\text{eff}}$  diagram.

There is a simple reason for the lack of detection of g-mode frequency peaks in p-mode stars observed from the ground. Because of daily gaps in ground-based photometry, night-to-night

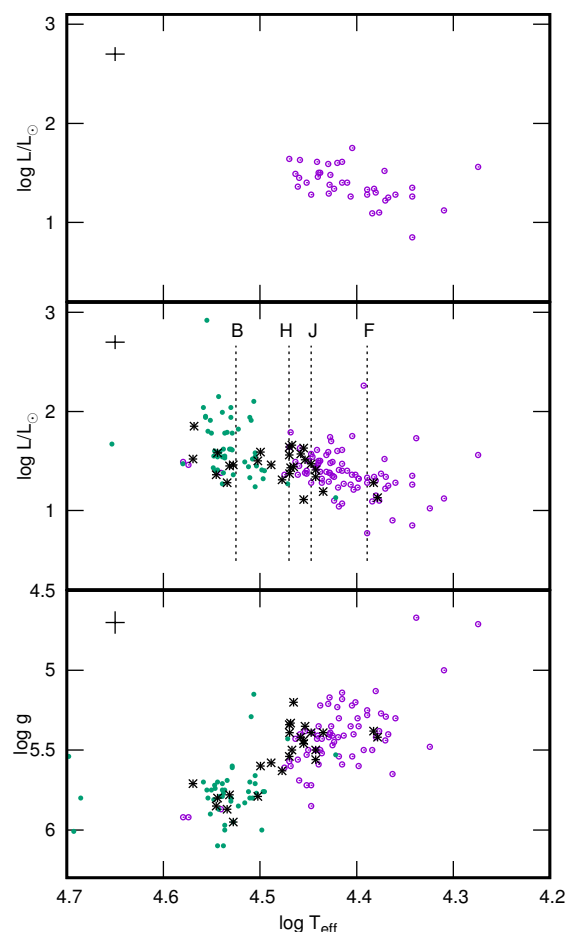


**Fig. 4.** Theoretical H–R diagram for *TESS* pulsating subdwarfs (top panel). Middle panel: All pulsating subdwarfs, including the *TESS* pulsators. The p-mode pulsators are shown as green filled circles and the g-mode pulsators as violet open circles. The hybrid pulsators are shown as black asterisks. The four dotted lines show the predicted hot limit of Fontaine et al. (2003) (F), Jeffery & Saio (2006) (J), Hu et al. (2009) (H), and Bloemen et al. (2014) (B). Bottom panel: Gravity–effective temperature diagram for all pulsating subdwarfs. The cross at the top left of each panel shows the approximate  $1\sigma$  error bars.

changes in atmospheric conditions and low amplitudes, low frequencies in the periodogram are contaminated by the daily alias peaks and instrumental drift. High frequency p-mode pulsations remain relatively unaffected. On the other hand, the almost continuous time sequences over many weeks obtained by *TESS* eliminates the aliasing problem and allows detection of low-frequency pulsations even at very low amplitudes.

There are three very hot g-mode pulsators among the p-mode stars in Fig. 4: TIC 442482669 (LS IV-14 116, Ahmad & Jeffery 2005), TIC 20420376 (UVO 0825+15, Jeffery et al. 2017), and TIC 371813244 (Feige 46, Latour et al. 2019). These pulsators may represent a different type of object (Dorsch et al. 2020).

## 7. Conclusions

A list of all known pulsating sdB stars was compiled by Holdsworth et al. (2017). This list was extended by a literature search, supplemented with the lists from Van Grootel et al. (2021) and presented in Table A1.

By cross-matching the positions of stars observed by *TESS* with the lists of subdwarf candidates by Geier (2020), a total of

1398 stars with *TESS* light curves was obtained. Using the stellar luminosities derived from *Gaia* parallaxes, stars not likely to be hot subdwarfs were identified and removed from the sample.

The periodograms of these stars were inspected and stars classified according to variability type. Pulsating hot subdwarfs are identified by the presence of multiple peaks in the periodogram. Many other stars showing only one peak below  $30 \text{ d}^{-1}$ , or one peak and its harmonics, are assumed to be binaries.

In this way, 63 pulsating hot subdwarfs were detected, 38 of which are listed in Van Grootel et al. (2021), but not classified as pulsating variables. The remaining 25 stars are previously unknown pulsating hot subdwarf candidates. This is a significant increase in the number of pulsating subdwarfs presented by the WG8 work. The new variables are presented in Tables A2 and A3. Their periodograms are shown in Figs. A1 and A2.

Stellar masses of a large sample of hot subdwarfs were determined from  $T_{\text{eff}}$ ,  $\log g$ , and  $\log L/L_{\odot}$ . Applying this method to a sample of p-mode and g-mode pulsators, it is found that masses of p-mode pulsators are 15 % higher than those of g-mode pulsators. The same result is found using asteroseismic masses.

While current pulsation models are able to explain the pulsations in these stars, they are unable to fix the location of the g-mode blue edge. The models by Bloemen et al. (2014) allow g-mode pulsations to continue well past the observed blue edge, depending on the amount of iron-group metal abundances in the driving zone.

The *TESS* observations have detected many stars with g-modes previously thought to be pure p-mode pulsators. As a result, these newly classified hybrid stars no longer form a tight group between the p- and g-mode stars. It seems likely that the previous observations could not detect the long periods of the g-mode stars, giving a misleading indication of the location of the hybrid stars. The situation is analogous to the lack of long-period detections from the ground in  $\delta$  Scuti stars. Space observations later showed that long periods (low frequencies) are present in almost all  $\delta$  Scuti variables (Balona 2014).

*Acknowledgements.* LAB thanks the National Research Foundation of South Africa for financial support. This paper includes data collected by the *TESS* mission. Funding for the *TESS* mission is provided by the NASA Explorer Program. Funding for the *TESS* Asteroseismic Science Operations Centre is provided by the Danish National Research Foundation (Grant agreement no.: DNR106), ESA PRODEX (PEA 4000119301) and Stellar Astrophysics Centre (SAC) at Aarhus University. We thank the *TESS* and TASC/TASOC teams for their support of the present work. This work has made use of data from the European Space Agency (ESA) mission *Gaia* (<https://www.cosmos.esa.int/gaia>), processed by the *Gaia* Data Processing and Analysis Consortium (DPAC, <https://www.cosmos.esa.int/web/gaia/dpac/consortium>). Funding for the DPAC has been provided by national institutions, in particular the institutions participating in the *Gaia* Multilateral Agreement. This research has made use of the SIMBAD database, operated at CDS, Strasbourg, France. This research has made use of the Vizier catalogue access tool, CDS, Strasbourg, France (DOI: 10.26093/cds/vizier). The original description of the Vizier service was published in A&AS 143, 23. The data presented in this paper were obtained from the Mikulski Archive for Space Telescopes (MAST). STScI is operated by the Association of Universities for Research in Astronomy, Inc., under NASA contract NAS5-2655.

## References

Ahmad, A. & Jeffery, C. S. 2005, A&A, 437, L51  
 Anders, F., Khalatyan, A., Chiappini, C., et al. 2019, A&A, 628, A94  
 Arentsen, A., Prugniel, P., Gonneau, A., et al. 2019, A&A, 627, A138  
 Arkhipova, V. P., Ikonnikova, N. P., Komissarova, G. V., & Esipov, V. F. 2002, Astronomy Letters, 28, 778  
 Bachulski, S., Baran, A. S., Jeffery, C. S., et al. 2016, Acta Astron., 66, 455  
 Bai, Y., Liu, J., Wicker, J., et al. 2018, ApJS, 235, 16  
 Balona, L. A. 2014, MNRAS, 437, 1476  
 Baran, A. S., Østensen, R. H., Telting, J. H., et al. 2018, MNRAS, 481, 2721

Baran, A. S., Reed, M. D., Østensen, R. H., Telting, J. H., & Jeffery, C. S. 2017, A&A, 597, A95  
 Bertelli, G., Girardi, L., Marigo, P., & Nasi, E. 2008, A&A, 484, 815  
 Bloemen, S., Hu, H., Aerts, C., et al. 2014, A&A, 569, A123  
 Borucki, W. J., Koch, D., Basri, G., et al. 2010, Science, 327, 977  
 Charpinet, S., Brassard, P., Fontaine, G., et al. 2019, A&A, 632, A90  
 Charpinet, S., Fontaine, G., Brassard, P., & Dorman, B. 1996, ApJ, 471, L103+  
 Côrsico, A. H., Uzundag, M., Kepler, S. O., et al. 2021, A&A, 645, A117  
 Dorman, B., Rood, R. T., & O'Connell, R. W. 1993, ApJ, 419, 596  
 Dorsch, M., Latour, M., Heber, U., et al. 2020, A&A, 643, A22  
 Dziembowski, W. A., Moskalik, P., & Pamyatnykh, A. A. 1993, MNRAS, 265, 588  
 Edelmann, H., Heber, U., Hagen, H. J., et al. 2003, A&A, 400, 939  
 Fontaine, G., Brassard, P., Charpinet, S., et al. 2003, ApJ, 597, 518  
 Fontaine, G., Brassard, P., Charpinet, S., et al. 2012, A&A, 539, A12  
 Gaia Collaboration, Brown, A. G. A., Vallenari, A., et al. 2018, A&A, 616, A1  
 Gaia Collaboration, Prusti, T., de Bruijn, J. H. J., et al. 2016, A&A, 595, A1  
 Geier, S. 2013, A&A, 549, A110  
 Geier, S. 2020, A&A, 635, A193  
 Geier, S., Heber, U., Edelmann, H., et al. 2013, A&A, 557, A122  
 Geier, S., Kupfer, T., Heber, U., et al. 2015, A&A, 577, A26  
 Geier, S., Østensen, R. H., Nemeth, P., et al. 2017a, A&A, 600, A50  
 Geier, S., Østensen, R. H., Nemeth, P., et al. 2017b, Open Astronomy, 26, 164  
 Geier, S., Raddi, R., Gentile Fusillo, N. P., & Marsh, T. R. 2019, A&A, 621, A38  
 Girven, J., Gänsicke, B. T., Steeghs, D., & Koester, D. 2011, MNRAS, 417, 1210  
 Gontcharov, G. A. 2017, Astronomy Letters, 43, 472  
 Gontcharov, G. A., Bajkova, A. T., Fedorov, P. N., & Akhmetov, V. S. 2011, MNRAS, 413, 1581  
 Green, E. M., Fontaine, G., Hyde, E. A., For, B. Q., & Chayer, P. 2008, in Astronomical Society of the Pacific Conference Series, Vol. 392, Hot Subdwarf Stars and Related Objects, ed. U. Heber, C. S. Jeffery, & R. Napiwotzki, 75  
 Green, E. M., Fontaine, G., Reed, M. D., et al. 2003, ApJ, 583, L31  
 Han, Z., Podsiadlowski, P., Maxted, P. F. L., & Marsh, T. R. 2003, MNRAS, 341, 669  
 Han, Z., Podsiadlowski, P., Maxted, P. F. L., Marsh, T. R., & Ivanova, N. 2002, MNRAS, 336, 449  
 Heber, U. 1986, A&A, 155, 33  
 Heber, U. 2009, ARA&A, 47, 211  
 Heber, U. 2016, PASP, 128, 082001  
 Heber, U., Hunger, K., Jonas, G., & Kudritzki, R. P. 1984, A&A, 130, 119  
 Heber, U., Werner, K., & Drilling, J. S. 1988, A&A, 194, 223  
 Hilditch, R. W., Harries, T. J., & Hill, G. 1996, MNRAS, 279, 1380  
 Holberg, J. B., Barstow, M. A., & Sion, E. M. 1998, ApJS, 119, 207  
 Holdsworth, D. L., Østensen, R. H., Smalley, B., & Telting, J. H. 2017, MNRAS, 466, 5020  
 Holdsworth, D. L., Smalley, B., Gillon, M., et al. 2014, MNRAS, 439, 2078  
 Hu, H., Nelemans, G., Aerts, C., & Dupret, M. 2009, A&A, 508, 869  
 Humason, M. L. & Zwicky, F. 1947, ApJ, 105, 85  
 Iben, I., J. & Tutukov, A. V. 1984, ApJ, 284, 719  
 Jeffery, C. S., Baran, A. S., Behara, N. T., et al. 2017, MNRAS, 465, 3101  
 Jeffery, C. S. & Saio, H. 2006, MNRAS, 372, L48  
 Jenkins, J. M., Twicken, J. D., McCauliff, S., et al. 2016, in Proc. SPIE, Vol. 9913, Software and Cyberinfrastructure for Astronomy IV, 99133E  
 Johnson, C., Green, E., Wallace, S., et al. 2014, in Astronomical Society of the Pacific Conference Series, Vol. 481, 6th Meeting on Hot Subdwarf Stars and Related Objects, ed. V. van Grootel, E. Green, G. Fontaine, & S. Charpinet, 153  
 Kawaler, S. D., Reed, M. D., Østensen, R. H., et al. 2010a, MNRAS, 409, 1509  
 Kawaler, S. D., Reed, M. D., Quint, A. C., et al. 2010b, MNRAS, 409, 1487  
 Kepler, S. O., Pelisoli, I., Koester, D., et al. 2015, MNRAS, 446, 4078  
 Kepler, S. O., Pelisoli, I., Koester, D., et al. 2016, MNRAS, 455, 3413  
 Kepler, S. O., Pelisoli, I., Koester, D., et al. 2019, MNRAS, 486, 2169  
 Kilkenny, D., Heber, U., & Drilling, J. S. 1988, South African Astronomical Observatory Circular, 12, 1  
 Kilkenny, D., Koen, C., O'Donoghue, D., & Stobie, R. S. 1997, MNRAS, 285, 640  
 Kilkenny, D., Luvhimb, E., O'Donoghue, D., et al. 1995, MNRAS, 276, 906  
 Kilkenny, D., Worters, H. L., & Lynas-Gray, A. E. 2019, MNRAS, 485, 4330  
 Kilkenny, D., Worters, H. L., & Østensen, R. H. 2017, MNRAS, 467, 3963  
 Koen, C., Kilkenny, D., O'Donoghue, D., van Wyk, F., & Stobie, R. S. 1997, MNRAS, 285, 645  
 Kupfer, T., Geier, S., Heber, U., et al. 2015, A&A, 576, A44  
 Lanz, T., Brown, T. M., Sweigart, A. V., Hubeny, I., & Landsman, W. B. 2004, ApJ, 602, 342  
 Latour, M., Green, E. M., & Fontaine, G. 2019, A&A, 623, L12  
 Lei, Z., Zhao, J., Németh, P., & Zhao, G. 2018, ApJ, 868, 70  
 Lei, Z., Zhao, J., Németh, P., & Zhao, G. 2019, ApJ, 881, 135  
 Luo, Y., Németh, P., Deng, L., & Han, Z. 2019, ApJ, 881, 7  
 Luo, Y.-P., Németh, P., Liu, C., Deng, L.-C., & Han, Z.-W. 2016, ApJ, 818, 202  
 Lynas-Gray, A. E. 2021, Frontiers in Astronomy and Space Sciences, 8, 19

- Maxted, P. F. L., Heber, U., Marsh, T. R., & North, R. C. 2001, *MNRAS*, 326, 1391
- Migliò, A., Montalbán, J., & Dupret, M.-A. 2007, *MNRAS*, 375, L21
- Miller Bertolami, M. M., Althaus, L. G., Unglaub, K., & Weiss, A. 2008, *A&A*, 491, 253
- Moehler, S., Heber, U., & de Boer, K. S. 1990, *A&A*, 239, 265
- Moni Bidin, C., Casetti-Dinescu, D. I., Girard, T. M., et al. 2017, *MNRAS*, 466, 3077
- Moskalik, P. & Dziembowski, W. A. 1992, *A&A*, 256, L5
- Napiwotzki, R. 2008, in *Astronomical Society of the Pacific Conference Series*, Vol. 391, *Hydrogen-Deficient Stars*, ed. A. Werner & T. Rauch, 257
- Németh, P., Kawka, A., & Vennes, S. 2012, *MNRAS*, 427, 2180
- O'Donoghue, D., Koen, C., Solheim, J. E., et al. 1998, *MNRAS*, 296, 296
- Oreiro Rey, R., Rodríguez López, C., Ulla, A., et al. 2004, in *Lecture Notes and Essays in Astrophysics*, ed. A. Ulla & M. Manteiga, Vol. 1, 133–142
- Østensen, R. H. 2006, *Baltic Astronomy*, 15, 85
- Østensen, R. H. 2012, in *Astronomical Society of the Pacific Conference Series*, Vol. 452, *Fifth Meeting on Hot Subdwarf Stars and Related Objects*, ed. D. Kilkenny, C. S. Jeffery, & C. Koen, 233
- Østensen, R. H., Jeffery, C. S., Saio, H., et al. 2020, *MNRAS*, 499, 3738
- Østensen, R. H., Oreiro, R., Solheim, J.-E., et al. 2010a, *A&A*, 513, A6
- Østensen, R. H., Silvotti, R., Charpinet, S., et al. 2011, *MNRAS*, 414, 2860
- Østensen, R. H., Silvotti, R., Charpinet, S., et al. 2010b, *MNRAS*, 409, 1470
- Pecaut, M. J. & Mamajek, E. E. 2013, *ApJS*, 208, 9
- Pelisolì, I., Vos, J., Geier, S., Schaffenroth, V., & Baran, A. S. 2020, *A&A*, 642, A180
- Pérez-Fernández, E., Ulla, A., Solano, E., Oreiro, R., & Rodrigo, C. 2016, *MNRAS*, 457, 3396
- Prugniel, P., Vauglin, I., & Koleva, M. 2011, *A&A*, 531, A165
- Ramspeck, M., Heber, U., & Edelmann, H. 2001, *A&A*, 379, 235
- Randall, S. K., Calamida, A., Fontaine, G., Bono, G., & Brassard, P. 2011, *ApJ*, 737, L27
- Randall, S. K., Calamida, A., Fontaine, G., et al. 2016, *A&A*, 589, A1
- Rauch, T., Heber, U., Hunger, K., Werner, K., & Neckel, T. 1991, *A&A*, 241, 457
- Reed, M. D., Armbrrecht, E. L., Telting, J. H., et al. 2018a, *MNRAS*, 474, 5186
- Reed, M. D., Baran, A. S., Telting, J. H., et al. 2018b, *Open Astronomy*, 27, 157
- Reed, M. D., Kawaler, S. D., Østensen, R. H., et al. 2010, *MNRAS*, 409, 1496
- Reed, M. D., O'Toole, S. J., Terndrup, D. M., et al. 2007, *ApJ*, 664, 518
- Reed, M. D., Shoaf, K. A., Németh, P., et al. 2020, *MNRAS*, 493, 5162
- Reed, M. D., Telting, J. H., Ketzner, L., et al. 2019, *MNRAS*, 483, 2282
- Ricker, G. R., Winn, J. N., Vanderspek, R., et al. 2014, in *Society of Photo-Optical Instrumentation Engineers (SPIE) Conference Series*, Vol. 9143, *Space Telescopes and Instrumentation 2014: Optical, Infrared, and Millimeter Wave*, ed. J. Oschmann, Jacobus M., M. Clampin, G. G. Fazio, & H. A. MacEwen, 914320
- Ritter, H. & Kolb, U. 2004, *VizieR Online Data Catalog*, V/113C
- Rodríguez-López, C., Lynas-Gray, A. E., Kilkenny, D., et al. 2010, *MNRAS*, 401, 23
- Saffer, R. A., Bergeron, P., Koester, D., & Liebert, J. 1994, *ApJ*, 432, 351
- Sahoo, S. K., Baran, A. S., Heber, U., et al. 2020a, *MNRAS*, 495, 2844
- Sahoo, S. K., Baran, A. S., Sanjayan, S., & Ostrowski, J. 2020b, *MNRAS*, 499, 5508
- Saio, H. & Jeffery, C. S. 2000, *MNRAS*, 313, 671
- Sánchez-Blázquez, P., Peletier, R. F., Jiménez-Vicente, J., et al. 2006, *MNRAS*, 371, 703
- Schaffenroth, V., Geier, S., Heber, U., et al. 2018, *A&A*, 614, A77
- Silvotti, R., Baran, A. S., Németh, P., et al. 2021, "submitted, 508, 869
- Silvotti, R., Uzundag, M., Baran, A. S., et al. 2019, *MNRAS*, 489, 4791
- Slettebak, A. & Brundage, R. K. 1971, *AJ*, 76, 338
- Soubiran, C., Le Campion, J.-F., Brouillet, N., & Chemin, L. 2016, *A&A*, 591, A118
- Stassun, K. G., Oelkers, R. J., Paegert, M., et al. 2019, *AJ*, 158, 138
- Stroerer, A., Heber, U., Lisker, T., et al. 2007, *A&A*, 462, 269
- Tian, Z., Liu, X., Yuan, H., et al. 2020, *ApJS*, 249, 22
- Uzundag, M., Vuckovic, M., Németh, P., et al. 2021, *arXiv e-prints*, arXiv:2105.15137
- Van Grootel, V., Charpinet, S., Brassard, P., Fontaine, G., & Green, E. M. 2013, *A&A*, 553, A97
- Van Grootel, V., Pozuelos, F. J., Thuillier, A., et al. 2021, *A&A*, 650, A205
- Vennes, S., Kawka, A., & Németh, P. 2011, *MNRAS*, 410, 2095
- Vos, J., Østensen, R. H., Németh, P., et al. 2013, *A&A*, 559, A54
- Wang, L., Gies, D. R., Peters, G. J., et al. 2021, *The Astronomical Journal*, 161, 248
- Webbink, R. F. 1984, *ApJ*, 277, 355
- Wenger, M., Ochsenbein, F., Egret, D., et al. 2000, *A&AS*, 143, 9
- Woudt, P. A., Warner, B., & Kilkenny, D. 2007, in *Astronomical Society of the Pacific Conference Series*, Vol. 372, *15th European Workshop on White Dwarfs*, ed. R. Napiwotzki & M. R. Burleigh, 619

## Appendix: Notes, tables and periodograms

This appendix gives an updated list of known pulsating subdwarfs in Table A1, which continues the list presented in Holdsworth et al. (2017). Table A2 presents the *TESS* stars listed in Van Grootel et al. (2021) that are unrecognised new pulsating variables. Periodograms of these stars are shown in Fig. A1. Table A3 presents additional new *TESS* pulsating variables. The periodograms of these stars are shown in Fig. A2.

### Notes to Table A2

**TIC 21343832.** A flare at BJD 2458844.77 seems to be present.

**TIC 63208546.** A peak at  $3.375 \text{ d}^{-1}$  with a very strong harmonic suggests a double-wave light curve with period  $P = 0.296 \text{ d}$  from orbital motion.

**TIC 151641733.** Pelisoli et al. (2020) attributed the peak at  $1.79 \text{ d}^{-1}$  as being due to rotation of the secondary. However, there are several peaks in the range  $22.7\text{--}29.7 \text{ d}^{-1}$  with S/N between 6 and 7 which are likely g-mode pulsations.

**TIC 201251043, 457225725.** These stars were analysed by Sahoo et al. (2020b) using *TESS* full-frame images sampled with a cadence of 30 min. Although they are listed as pulsating sdB stars, the long cadence prohibits the detection of frequencies higher than about  $24 \text{ d}^{-1}$ . They all have frequency peaks exceeding this limit.

**TIC 279373920.** A high-amplitude peak at  $2.126 \text{ d}^{-1}$  and its harmonic indicates binary motion with  $P = 0.468 \text{ d}$ .

**TIC 311432346.** The light curve shows clear sinusoidal variations with a period  $P = 1.495 \text{ d}$ , which is perhaps orbital.

**TIC 311898870.** The main frequency peak and a marginal harmonic suggest orbital motion with  $P = 0.363 \text{ d}$ .

**TIC 380641758.** The pulsation frequencies in this star do not correspond to those generally seen in sdB or sdO stars. Typical sdO pulsations are in the p-mode region, which is higher than the *TESS* Nyquist frequency. Perhaps they originate in the A-type companion.

**TIC 421895532.** A peak at  $1.314 \text{ d}^{-1}$  and its harmonic indicates binary motion with  $P = 0.761 \text{ d}$ . The harmonic to the main peak at  $6.896 \text{ d}^{-1}$  is also present. Perhaps  $0.761 \text{ d}$  represents rotation and  $0.145 \text{ d}$  the orbital motion.

**TIC 466277784.** The strongest peak at  $1.667 \text{ d}^{-1}$  and its harmonic suggests binary motion with period  $P = 0.599 \text{ d}$ .

### Notes to Table A3

**TIC 23838673.** A forest of frequencies below  $10 \text{ d}^{-1}$  indicate a main sequence  $\beta\text{Cep}$ . There is a cut-off frequency limit for sdBV pulsation mode excitation (about  $5 \text{ d}^{-1}$ ) below which we do not see any pulsation due to energy dispersion in the driving zone. However, in this star there are some higher frequency modes of low amplitudes visible in the periodogram, and we left it for further investigations.

**TIC 56541907.** The presence of a strong peak at  $7.770 \text{ d}^{-1}$  and its harmonic suggest a binary with period  $P = 0.129 \text{ d}$ .

**TIC 124802885 (HD 154137) and TIC 301776333 (HD 289333).** While both are classified as normal main sequence stars, their luminosities are well within the hot subdwarf range. They are not listed as subdwarf candidates in the literature. It is possible that the *Gaia* parallaxes are in error.

**TIC 176089274.** The peak at  $5.608 \text{ d}^{-1}$  has a weak harmonic suggesting orbital motion with  $P = 0.178 \text{ d}$ .

**TIC 219641382.** The light curve shows a clear sinusoidal variation with  $P = 2.7 \text{ d}$ .

**TIC 224284872.** This high-latitude faint star is listed as a candidate hot subdwarf in Geier et al. (2019) and also in Gontcharov et al. (2011). The luminosity is certainly compatible with a subdwarf (no reliable effective temperature has been measured). However, it was given an A0 classification by Slettebak & Brundage (1971) and listed as a high-frequency A-type main sequence pulsator by Holdsworth et al. (2014). On the basis of the low luminosity it is a likely V1093 Her star with a rich frequency spectrum in the range  $50\text{--}130 \text{ d}^{-1}$ . There are several interesting relationships between frequencies that suggest tidal interaction in a binary system. The presence of a peak at  $0.734 \text{ d}^{-1}$  and its high-amplitude harmonic can be seen as a double-wave variation in the light curve. This could be a result of binary motion with period  $P = 1.362 \text{ d}$ . The star might turn out to be a main sequence star with incorrect parallax, but it certainly deserves attention.

**TIC 262753627.** The star was also analysed by Sahoo et al. (2020b) using *TESS* full-frame images sampled with a cadence of 30 min. It is not listed in Van Grootel et al. (2021).

**TIC 282810113.** While the single peak at  $13.001 \text{ d}^{-1}$  is present, there are four other peaks with  $4 < \text{S/N} < 5$ . However, confirmation of these frequencies is clearly required.

**TIC 314296949** High amplitude frequencies in the range  $5\text{--}10 \text{ d}^{-1}$  are unusual in an sdBV star.

**TIC 471013511** The only significant peak at  $10.25 \text{ d}^{-1}$  may be due to low-amplitude binary variations, either rotation or pulsation. While it is listed as a cataclysmic binary or related object by Ritter & Kolb (2004), it lies well within the sdB instability strip among the g-mode pulsators.



**Table A1.** Pulsating hot subdwarfs discovered since Holdsworth et al. (2017). The pulsation type is either P (p-mode), G (g-mode), or H (both p- and g-modes present). Suspected binary systems are labelled B. The effective temperature (kK) and luminosity (from *Gaia* EDR3 parallaxes) are shown. If no value of  $T_{\text{eff}}$  is available, the calculation of the luminosity assumes  $T_{\text{eff}} = 3.0$  kK. The surface gravity,  $\log(g)$ , and the log helium abundance  $Y = n(\text{He})/n(\text{H})$  are from Geier (2020). The reference codes for pulsation (Pref) and for the effective temperatures (Tref) are listed in the last two columns. The second half of the table lists the *TESS* sdBV stars discovered by Van Grootel et al. (2021).

TIC	Name	Type	$T_{\text{eff}}$ (kK)	$\log(L/L_{\odot})$	$\log(g)$	$\log(Y)$	Pref	Tref
-	DENIS J231105.0-013705	P	$35.35 \pm 0.60$	$1.43 \pm 0.16$			42	31,42
2621707	SDSS J135544.71-080354.3	G	$27.00 \pm 0.20$	$1.39 \pm 0.10$			20	13,20,22
13145616	CD-28 1974	G	$29.84 \pm 0.50$	$1.36 \pm 0.07$	$5.61 \pm 0.06$	$-2.44 \pm 0.14$	40	12,14,40
20420376	UVO 0825+15	G	$37.98 \pm 0.40$	$1.49 \pm 0.07$	$5.92 \pm 0.10$	$-0.62 \pm 0.08$	24	14,19,24,26
20448010	EC 11119-2405	G	$23.43 \pm 0.48$	$1.34 \pm 0.07$	$5.29 \pm 0.08$	$-2.46 \pm 0.31$	43	14,43
21223262	SDSS J083603.98+155216.4	G	$26.24 \pm 0.50$	$1.23 \pm 0.09$	$5.42 \pm 0.07$	$-2.45 \pm 0.17$	27	13,21,22,29,33
60257911	SDSS J082003.35+173914.2	P	$36.00 \pm 2.00$	$1.94 \pm 0.09$			27	27
67584818	CD-33 417	G	$25.06 \pm 0.50$	$1.23 \pm 0.07$	$5.30 \pm 0.20$	$-2.80 \pm 0.00$	41	1,3,41
71013467	EC 04205-1328	G		$2.32 \pm 0.07$			39	
117070953	TIC 117070953	H	$170.00 \pm 2.00$	$1.76 \pm 0.07$			25	45
137608661	TYC 4544-2658-1	B+G	$27.30 \pm 0.20$	$1.40 \pm 0.07$	$5.39 \pm 0.04$	$-2.95 \pm 0.05$	46	46
138707823	Ton S 135	G	$25.00 \pm 0.30$	$1.32 \pm 0.07$	$5.60 \pm 0.20$	$-2.30 \pm 0.20$	43	2,15,43
139723188	EC 21811-5010	P	$35.00 \pm 4.00$	$1.54 \pm 0.09$			35	35
156618553	HW Vir	H	$30.00 \pm 0.60$	$1.31 \pm 0.07$	$5.63 \pm 0.05$	$0.00 \pm 0.00$	28	6,17
169285097	SB 815	H	$27.20 \pm 0.55$	$1.25 \pm 0.05$	$5.39 \pm 0.10$	$-2.94 \pm 0.01$	41	1,14,41
180205000	EC 11545-1459	P	$34.00 \pm 2.00$	$1.62 \pm 0.14$			35	35
195189122	LB 378	P	$35.24 \pm 0.60$	$1.60 \pm 0.13$	$5.72 \pm 0.11$	$-1.92 \pm 0.19$	27	18,27,33,36
207440585	SDSS J161926.58+560558.6	P	$33.90 \pm 0.50$	$1.94 \pm 0.07$	$5.80 \pm 0.00$	$-1.60 \pm 0.00$	9	10
220573709	EC 03089-6421	P	$52.00 \pm 3.00$	$1.61 \pm 0.07$			35	35
231846470	EC 01441-6605	P	$36.00 \pm 2.00$	$1.95 \pm 0.07$			35	35
233689607	TIC 233689607	G	$140.00 \pm 2.00$	$2.15 \pm 0.09$			25	45
260795163	EC 23073-6905	G	$27.00 \pm 0.50$	$1.56 \pm 0.07$			43	5,43
278659026	EC 21494-7018	G	$23.06 \pm 0.30$	$0.90 \pm 0.07$	$5.65 \pm 0.03$	$-3.22 \pm 1.15$	32	14,15
335635628	PG 1315-123	H	$37.00 \pm 1.00$	$1.85 \pm 0.37$			34	34
352444061	TIC 352444061	G		$1.70 \pm 0.08$			25	
371813244	Feige 46	G	$37.50 \pm 0.50$	$1.46 \pm 0.07$	$5.92 \pm 0.02$	$-0.50 \pm 0.02$	37	3,33,56,57
382518318	GALEX J075010.4-644617	G		$1.77 \pm 0.07$			39	
391825813	EC 10834-1301	P	$45.00 \pm 5.00$	$1.67 \pm 0.10$			35	35
397064286	GALEX J050735.7+034815	G	$23.99 \pm 0.63$	$1.15 \pm 0.07$	$5.42 \pm 0.11$	$-3.05 \pm 0.78$	44	14
415339307	HS 0352+1019	G	$25.00 \pm 0.50$	$1.32 \pm 0.07$	$5.35 \pm 0.10$	$-2.70 \pm 0.20$	43	7,26,43
418789164	HD 4539	H	$24.12 \pm 0.20$	$1.28 \pm 0.07$	$5.38 \pm 0.05$	$-2.42 \pm 0.20$	38	8,11,14,15,19,30
432223488	EC 15061-1442	P	$32.00 \pm 2.00$	$1.54 \pm 0.07$			35	35
437043466	SDSS J083612.03+191755.9	H	$29.47 \pm 0.20$	$1.37 \pm 0.07$	$5.39 \pm 0.20$	$-2.81 \pm 0.00$	23	14,21,23,26
446005482	TIC 446005482	G	$135.00 \pm 2.00$	$2.76 \pm 0.10$			25	49
452718256	EC 11275-2504	P	$38.00 \pm 2.00$	$1.47 \pm 0.07$			35	35
457168745	PG 0342+026	G	$26.00 \pm 1.00$	$1.07 \pm 0.07$	$5.59 \pm 0.12$	$-2.69 \pm 0.10$	41	4,15,16
9346617	KUV 09565+3632	G	$27.40 \pm 0.20$	$1.54 \pm 0.07$	$5.22 \pm 0.03$	$-2.69 \pm 0.08$	47	21,26
9358354	GALEX J045213.2-091634	G		$1.59 \pm 0.08$			47	
31959467	GALEX J191849.6-310441	G		$1.43 \pm 0.07$			47	
33834484	[DI91] 1569	G	$24.10 \pm 0.50$	$1.34 \pm 0.07$			47	53
56124677	SDSS J044246.86-071654.4	G	$22.00 \pm 0.50$	$1.26 \pm 0.08$			47	22
63719894	FBS 0212+334	G		$1.61 \pm 0.07$			47	
68873560	PG 1635+414	G	$26.85 \pm 0.42$	$1.29 \pm 0.07$	$5.42 \pm 0.06$	$-2.75 \pm 0.24$	47	14
80170223	BPS CS 22964-0098	G		$1.53 \pm 0.07$			47	
101817287	EC 20106-5248	G	$24.50 \pm 0.50$	$1.33 \pm 0.09$	$5.25 \pm 0.12$	$-2.77 \pm 0.10$	47	15,16
126659216	EC 20570-4308	G		$1.52 \pm 0.08$			47	
146323153	GALEX J045547.2-203417	G		$2.09 \pm 0.07$			47	
156623726	Ton 194	G	$27.60 \pm 1.00$	$1.61 \pm 0.08$	$5.43 \pm 0.15$	$-2.30 \pm 0.10$	47	50,58
158918567	TYC 3133-2416-1	G	$28.00 \pm 0.50$	$1.28 \pm 0.07$	$5.72 \pm 0.09$	$-2.44 \pm 0.16$	47	26,56,57
159734503	BPS CS 29501-0054	G		$1.58 \pm 0.08$			47	
178893906	EC 04284-2758	G		$1.45 \pm 0.07$			47	
220476769	EC 05012-5641	G		$1.71 \pm 0.09$			47	
234295068	EC 23483-6445	G		$1.51 \pm 0.07$			47	
261241692	EC 19269-6231	G		$1.62 \pm 0.08$			47	
279433960	BPS CS 22190-0004	G		$1.50 \pm 0.08$			47	
279826483	US 719	G		$1.58 \pm 0.07$			47	

TIC	Name	Type	$T_{\text{eff}}$ (kK)	$\log(L/L_{\odot})$	$\log(g)$	$\log(Y)$	Pref	Tref
283870336	Ton 245	G	$22.90 \pm 0.50$	$1.28 \pm 0.07$	$5.30 \pm 0.15$	$-2.50 \pm 0.10$	47	3,4
293165262	EC 04256-5912	G	$26.00 \pm 0.50$	$1.40 \pm 0.07$			47	53
298109741	PG 1340+607	G		$1.71 \pm 0.07$			47	
298542142	V* V1099 Her	G	$27.55 \pm 0.50$	$1.46 \pm 0.07$	$5.41 \pm 0.03$	$-2.70 \pm 0.07$	47	26
309658435	EC 05155-6100	G	$25.70 \pm 0.40$	$1.40 \pm 0.08$			47	53
309791758	EC 05201-6132	B+G		$1.54 \pm 0.08$			47	
317439554	KPD 0716+0258	G	$26.30 \pm 1.00$	$1.60 \pm 0.08$	$5.23 \pm 0.02$	$-2.46 \pm 0.10$	47	26
319602897	EC 19205-5916	G		$1.51 \pm 0.08$			47	
320660807	GALEX J194855.8-583737	G		$1.42 \pm 0.07$			47	
332742020	PG 0209-015	G	$23.50 \pm 0.50$	$1.52 \pm 0.08$			47	48
347435900	Ton 209	G	$29.50 \pm 1.00$	$1.64 \pm 0.07$	$5.57 \pm 0.15$	$-3.00 \pm 0.00$	47	3,4
352315023	JL 36	G	$24.00 \pm 0.50$	$1.30 \pm 0.07$	$5.13 \pm 0.16$	$-2.67 \pm 0.20$	47	3,5,4,57
369394241	HE 0452-3654	G		$1.48 \pm 0.07$			47	
388940683	PG 1230+052	G	$28.30 \pm 1.00$	$1.40 \pm 0.07$	$5.72 \pm 0.15$	$-3.00 \pm 0.10$	47	4
436682542	GALEX J045437.4+140125	G		$2.08 \pm 0.07$			47	
445927286	PG 0314+103	G					47	
455755305	FBS 2347+385	G	$23.80 \pm 0.50$	$1.10 \pm 0.07$	$5.38 \pm 0.06$	$-3.44 \pm 0.30$	47	14,17
471013461	EC 03530-4024	G		$1.63 \pm 0.08$			47	

1-Heber et al. (1984); 2-Heber (1986); 3-Kilkenny et al. (1988); 4-Saffer et al. (1994); 5-Kilkenny et al. (1995); 6-Hilditch et al. (1996); 7-Edelmann et al. (2003); 8-Sánchez-Blázquez et al. (2006); 9-Reed et al. (2007); 10-Østensen et al. (2010a); 11-Prugniel et al. (2011); 12-Vennes et al. (2011); 13-Girven et al. (2011); 14-Németh et al. (2012); 15-Geier (2013); 16-Geier et al. (2013); 17-Kupfer et al. (2015); 18-Kepler et al. (2015); 19-Soubiran et al. (2016); 20-Bachulski et al. (2016); 21-Luo et al. (2016); 22-Pérez-Fernández et al. (2016); 23-Baran et al. (2017); 24-Jeffery et al. (2017); 25-Córsico et al. (2021); 26-Lei et al. (2018); 27-Reed et al. (2018a); 28-Baran et al. (2018); 29-Reed et al. (2018b); 30-Arentsen et al. (2019); 31-Anders et al. (2019); 32-Charpinet et al. (2019); 33-Lei et al. (2019); 34-Reed et al. (2019); 35-Kilkenny et al. (2019); 36-Kepler et al. (2019); 37-Latour et al. (2019); 38-Silvotti et al. (2019); 39-Pelisolli et al. (2020); 40-Reed et al. (2020); 41-Sahoo et al. (2020a); 42-Østensen et al. (2020); 43-Uzundag et al. (2021); 44-Schaffenroth et al. (2018); 45-Holberg et al. (1998); 46-Silvotti et al. (2021); 47-Van Grootel et al. (2021).

**Table A2.** List of 38 newly discovered pulsating sdB stars not marked as pulsators in the Van Grootel et al. (2021) catalogue. The columns are the same as in Table A1. An asterisk refers to a note for the star. The column marked F gives the following flags: 1 - an isolated target or target star with neighbours that have no influence on the target fluxes; 2 - a crowded field where the target flux is not substantially polluted by light from neighbouring stars; 3 - a star with bright neighbours that might substantially affect the amplitudes of the subdwarf light variation. The last column is the spectral type from Van Grootel et al. (2021).

TIC	Name	Type	$T_{\text{eff}}$ (kK)	Tref	$\log(L/L_{\odot})$	$\log(g)$	$\log(Y)$	F	Type
21343832*	HS 0740+3734	G	$20.40 \pm 0.90$	7	$1.12 \pm 0.08$	$5.00 \pm 0.20$	$-2.10 \pm 0.40$	1	sdB
40050637	KUV 16256+4034	G	$23.46 \pm 0.50$	14,17,26	$1.22 \pm 0.07$	$5.44 \pm 0.07$	$-3.08 \pm 0.29$	2	sdB
63208546*	KIC 8754603	B+G		56	$1.25 \pm 0.07$	$6.09 \pm 0.02$	$-2.43 \pm 0.13$	2	sdB+?
70963660	EC 04178-1734	G			$1.40 \pm 0.07$			3	sdB
88484868	FBS 0658+627	G	$28.75 \pm 0.37$	14	$1.63 \pm 0.07$	$5.40 \pm 0.07$	$-2.76 \pm 0.26$	3	sdB
118298029	GALEX J021618.9+275900	G	$25.48 \pm 0.45$	14	$1.26 \pm 0.07$	$5.35 \pm 0.05$	$-2.81 \pm 0.23$	1	sdB
137502282	TIC 137502282	G			$1.39 \pm 0.07$			2	B1,sdB
151641733*	GALEX J110743.0-373158	G			$2.29 \pm 0.07$			2	sdB+MS
154510451	FBS 1224+780	G			$1.50 \pm 0.07$			1	sdB
199732600	HE 0127-43250	G			$1.57 \pm 0.08$			1	sdB
201251043*	TIC 201251043	G			$1.54 \pm 0.07$			1	sdB
202354658	PG 1544+601	G	$29.06 \pm 0.50$	14	$1.49 \pm 0.08$	$5.43 \pm 0.05$	$-3.44 \pm 0.60$	1	sdB
229706981	TIC 229706981	G			$1.58 \pm 0.11$			3	sdB
232521983	TYC 4407-187-1	G			$1.55 \pm 0.07$			1	sdB
233211303	HS 1747+6924	G	$27.50 \pm 1.20$	7	$1.50 \pm 0.08$	$5.35 \pm 0.20$	$-2.90 \pm 0.30$	1	sdB
240109525	GALEX J064347.7+320147	G	$26.88 \pm 0.50$	26	$1.59 \pm 0.08$	$5.21 \pm 0.01$	$-2.70 \pm 0.05$	3	sdB
240783347	TIC 240783347	G			$1.36 \pm 0.07$			1	sdB
269766236	TIC 269766236	G			$1.53 \pm 0.07$			1	sdB
273218137	TIC 273218137	G			$1.55 \pm 0.07$			3	sdB
274623605	PG 1700+48605	G	$26.01 \pm 1.11$	14	$1.61 \pm 0.07$	$5.18 \pm 0.09$	$-2.58 \pm 0.33$	3	sdB
279373920*	TIC 279373920	B+G			$1.51 \pm 0.07$			1	sdB
308179612	EC 13080-1508	G			$1.41 \pm 0.07$			1	sdB
311432346*	BD+29 3070	B+G	$25.38 \pm 0.99$	52	$1.75 \pm 0.07$	$5.54 \pm 0.18$	$-2.63 \pm 0.00$	1	sdB F
311898870*	FBS 2202+436	B+G			$1.41 \pm 0.07$			1	sdB
331553315	FBS 0430+772	G	$26.80 \pm 0.70$	7	$1.38 \pm 0.07$	$5.40 \pm 0.10$	$-3.00 \pm 0.20$	3	sdB
352412700	KUV 20417+7604	G			$1.55 \pm 0.07$			2	sdB
365496228	TIC 365496228	G	$22.00 \pm 1.00$	13	$0.85 \pm 0.07$			3	sdB
367003034	80 GALEX J223336.8+741254	G			$1.57 \pm 0.07$			2	sdB
380641758*	BD+10 2357	G			$2.06 \pm 0.07$			1	sdO+A
387107334	BPS CS 22959-0140	G			$1.47 \pm 0.08$			2	sdB
405799245	PG 0926+06545	G	$26.50 \pm 0.68$	14,26	$1.34 \pm 0.07$	$5.45 \pm 0.08$	$-2.79 \pm 0.46$	2	sdB
408552372	EC 12578-2107	G			$1.53 \pm 0.07$			1	sdB
421895532*	JL 111	B+G			$1.30 \pm 0.07$			1	sdB
424383364	HS 1831+7647	G	$23.30 \pm 0.60$	7	$1.25 \pm 0.07$	$5.40 \pm 0.10$	$-3.00 \pm 0.20$	3	sdB
437746793	PG 0011+283	G	$24.20 \pm 0.50$	33,56,57	$1.09 \pm 0.07$	$5.50 \pm 0.03$	$-4.05 \pm 0.28$	1	sdB
457225725*	TIC 457225725	G			$1.24 \pm 0.07$			1	sdB
466277784*	EC 20182-6534	B+G			$1.46 \pm 0.07$			1	sdB+WD
468980287	GALEX J083412.3+071211	G	$28.90 \pm 0.50$	13,14,26	$1.36 \pm 0.08$	$5.56 \pm 0.12$	$-2.62 \pm 0.00$	2	sdB

48-Moehler et al. (1990); 49-Ramspeck et al. (2001); 50-Maxted et al. (2001); 51-Arhipova et al. (2002); 52-Vos et al. (2013); 53-Moni Bidin et al. (2017); 54-Geier et al. (2017b); 55-Bai et al. (2018); 56-Luo et al. (2019); 57-Geier (2020); 58-Tian et al. (2020);

**Table A3.** List of 25 newly discovered *TESS* pulsating sdB candidates that are not listed in Van Grootel et al. (2021). The columns are the same as in Table A2. The last column is the spectral type from the literature.

TIC	Name	Type	$T_{\text{eff}}$ (kK)	$T_{\text{ref}}$	$\log(L/L_{\odot})$	$\log(g)$	$\log(Y)$	F	Type
23838673*	PG 1400+389	G	$18.80 \pm 1.00$	49	$1.56 \pm 0.07$	$4.71 \pm 0.10$	$-0.71 \pm 0.00$	1	sd:O
53826859	TIC 53826859	G			$2.02 \pm 0.09$			3	
56541907*	TIC 56541907	B+G			$1.55 \pm 0.07$			2	
71340025	GALEX J101850.0-333150	G			$1.56 \pm 0.07$			3	sdO/B
124802885*	HD 154137	G			$1.22 \pm 0.07$			3	
139481265	TIC 139481265	G			$1.22 \pm 0.07$			3	
153279970	TIC 153279970	G			$1.47 \pm 0.07$			3	
176089274*	TIC 176089274	B+G			$2.08 \pm 0.09$			3	
196278926	TIC 196278926	G			$1.31 \pm 0.07$			3	
219641382*	EC 11383-2238	B+G			$1.69 \pm 0.07$			2	sdB+MS
224284872*	SB 825	B+G			$1.60 \pm 0.07$			1	A3
262753627*	TIC 262753627	G	$28.80 \pm 0.50$	26,56,57	$1.45 \pm 0.07$	$5.69 \pm 0.02$	$-2.64 \pm 0.03$	3	
266200506	GALEX J075215.1+004711	G			$1.48 \pm 0.08$			3	sdB
282810113*	TIC 282810113	G			$1.73 \pm 0.07$			3	
301776333	HD 289333	G			$2.38 \pm 0.07$			3	B5
314296949*	TIC 314296949	G			$1.32 \pm 0.07$			3	
332841294	TIC 332841294	G			$1.48 \pm 0.07$			3	
345297807	PG 1444+236	G	$22.00 \pm 0.50$	51	$1.35 \pm 0.07$			1	sd
378898110	TIC 378898110	G			$0.59 \pm 0.07$			2	
384486510	CPD-79 906	G			$2.22 \pm 0.07$			1	B8
389175842	PG 0940+068	G	$26.74 \pm 1.00$	33,56	$1.48 \pm 0.08$	$5.39 \pm 0.04$	$-2.93 \pm 0.07$	3	sdB+WD,DA2:
396874449	PG 1111-077	G			$1.33 \pm 0.07$			1	sdOB
453168096	TIC 453168096	G			$-0.19 \pm 0.13$			2	
468912698	GALEX J075257.2+055911	G			$1.46 \pm 0.08$			3	sdB
471013511*	BPS CS 22879-0149	G	$24.50 \pm 0.50$	19	$1.28 \pm 0.08$			1	sdB

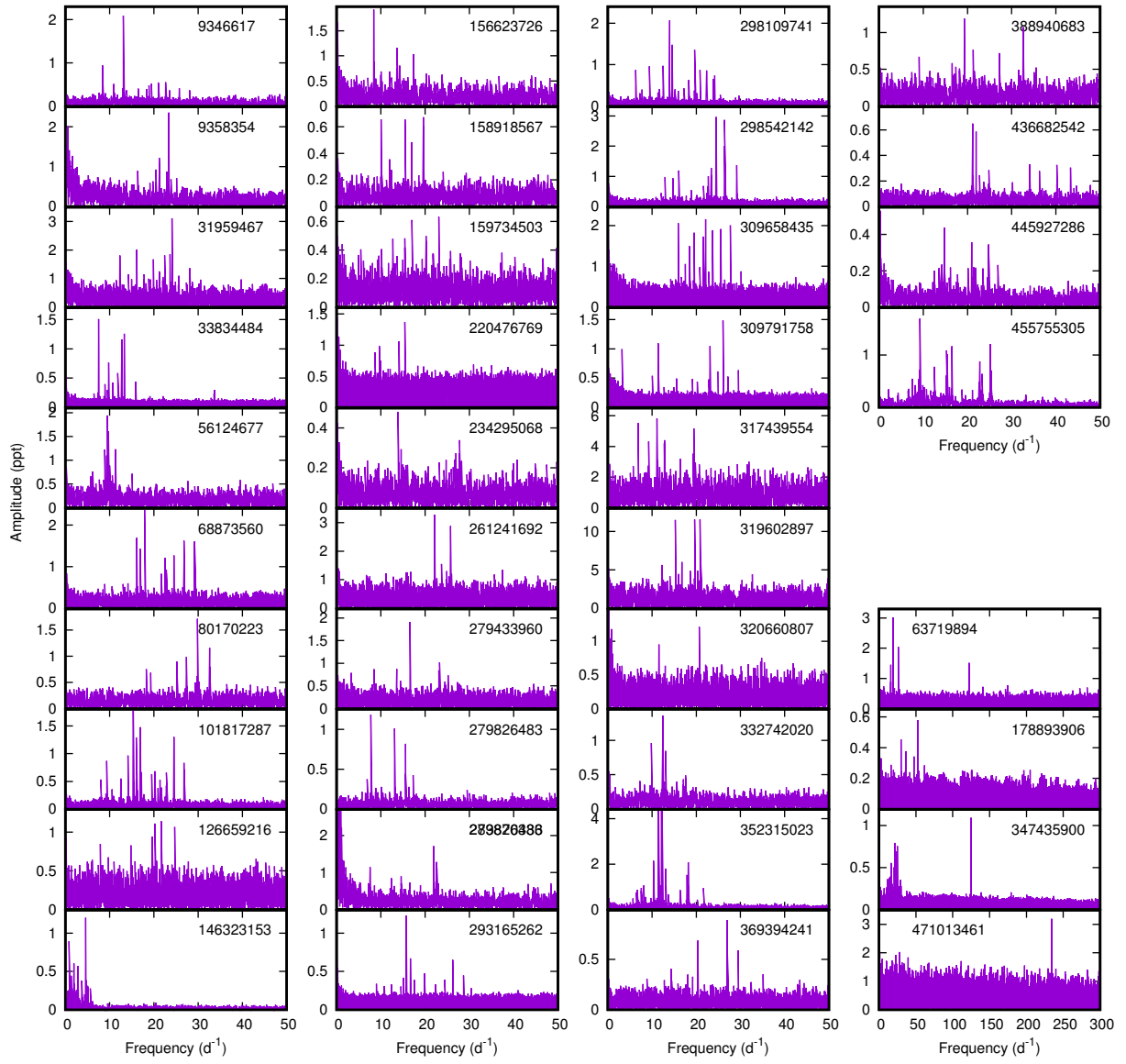


**Fig. A1.** Periodograms of unrecognised sdBV stars in Van Grootel et al. (2021). The amplitude is in parts per thousand.

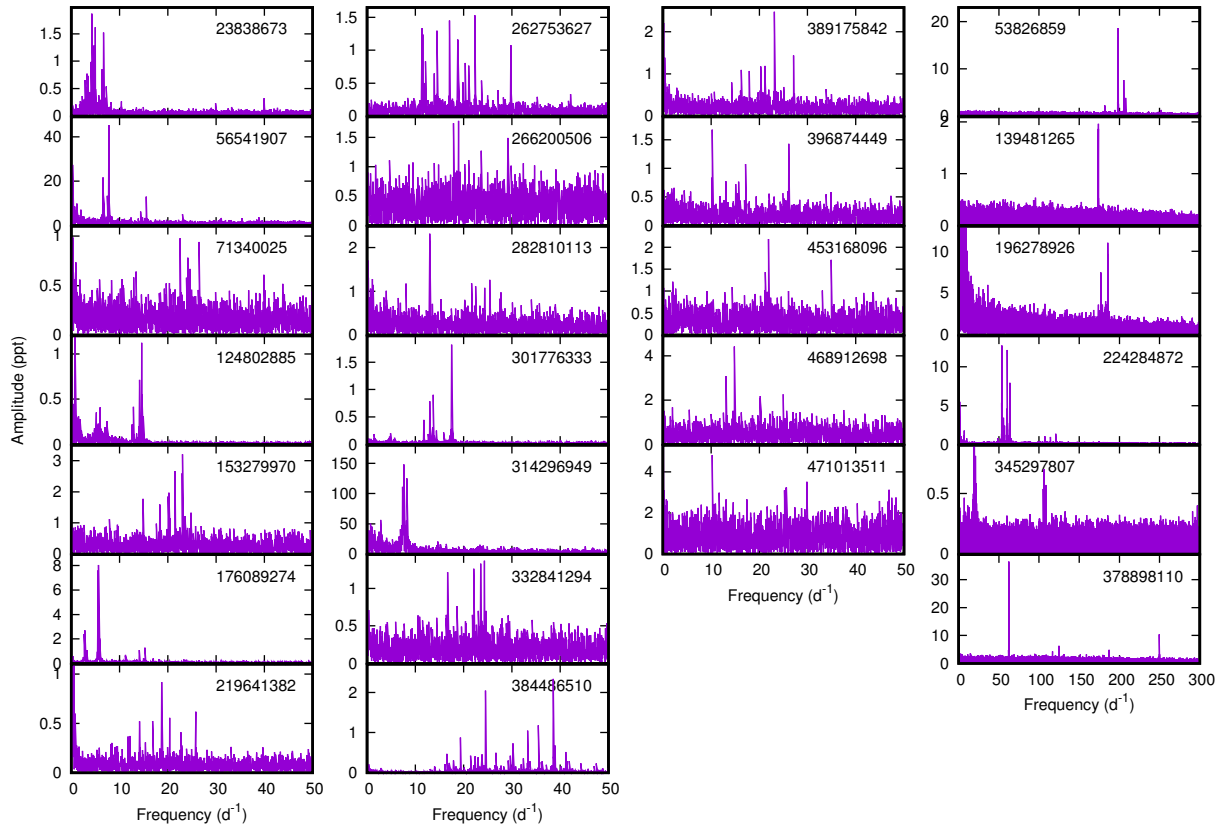


**Fig. A2.** Periodograms of newly discovered *TESS* sdBV stars. The amplitude is in parts per thousand.